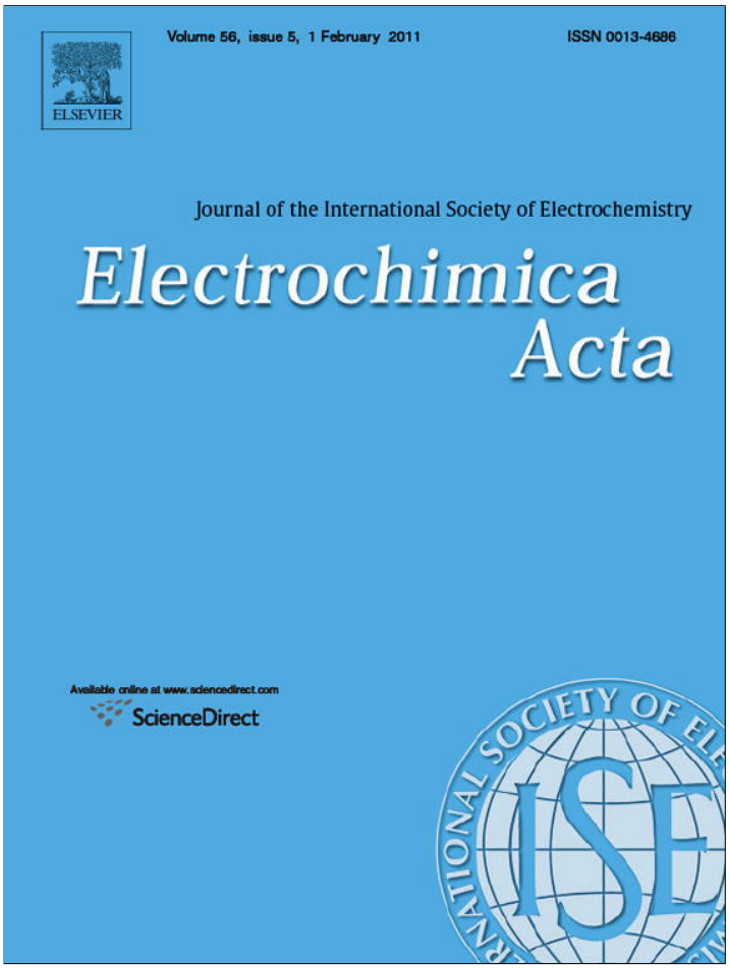

Electrochimica Acta 56 (2011) 2378–2384

Contents lists available at ScienceDirect

Electrochimica Acta

journal homepage: www.elsevier.com/locate/electacta

Tuning the microstructure and functional properties of metal nanowire arrays via deposition potential

Kirill S. Napolskii[a,*], Ilya V. Roslyakov[a], Andrey A. Eliseev[a], Dmitry I. Petukhov[a], Alexey V. Lukashin[a], Shu-Fang Chen[b], Chuan-Pu Liu[b], Galina A. Tsirlina[c,1]

[a] Department of Materials Science, Moscow State University, Leninskie Hills, 119991, Moscow, Russia
[b] Department of Materials Science and Engineering, National Cheng Kung University, 701, Tainan, Taiwan
[c] Department of Electrochemistry, Moscow State University, Leninskie Hills, 119991, Moscow, Russia

ARTICLE INFO

Article history:
Received 4 August 2010
Received in revised form 1 December 2010
Accepted 4 December 2010
Available online 15 December 2010

Keywords:
Anodic aluminum oxide
Nanowire array
Templated electrodeposition
Current transients
Coulometric analysis

ABSTRACT

The present study is focused on electrochemical fabrication and characterization of the ordered arrays of one-dimensional Ni nanostructures templated by porous anodic alumina films. A possibility to monitor and control homogeneity of arrays and completeness of the pores filling in the course of potentiostatic deposition is discussed. Current efficiency is determined from independent analytical data and taken into account in the treatment of charge transients. The crystallinity of Ni nanowire arrays as well as the homogeneity and completeness of the replication process are demonstrated to be controlled by deposition potential. Just these structural features affect the magnetic properties of nanowire arrays. The advantages and drawbacks of the quantitative coulometric analysis of current transients are considered.

1. Introduction

Template synthesis is known as a bottom-up approach, which is widely used for preparation of various types of nanostructures. As compared to the top-down techniques, such as X-ray or electron lithography, templated chemical and/or physicochemical fabrication methods are highly flexible, very fast and cheap pathways enabling large-scale preparation of uniform nanostructure arrays. These arrays, as well as well-characterized separate nanostructures, attract a great attention both from fundamental and practical points of view, acting as elementary blocks in a magnetic high-density storage devices [1,2], high efficiency emitters [3–5], sensors [6,7], etc.

Templates, also known as matrices, generally perform several functions. First, they play a role of structure directing agent and determine geometric parameters of the replicated object. In particular, uniform nanostructures can be fabricated only in templates possessing uniform porosity. Second, the matrix determines an arrangement of nanostructures in the array, allowing to construct nanocomposite material with a desired structure without lithography equipment. Finally, template enables one to protect nanoparticles from the effect of external factors (e.g., from oxidation in air).

The accuracy of template replication by the embedded material strongly depends on the incorporation technique. In most cases it is difficult to achieve a complete filling of a template with desired material. For instance, infiltration methods with subsequent decomposition of precursors usually result in formation of small clusters along the walls of the porous frameworks [8]. CVD related techniques can be successfully utilized for the incorporation of complex materials into the channels of porous media, but the problem of uniform filling of porous structure due to probable pore blocking by growing phases is still far from being resolved [9]. For insulating matrices, more promise is given by electrodeposition method which basically allows almost complete filling of the pores due to continuous movement of the growth front through porous structure. Another advantage of this approach appears when electrocrystallization takes place, which is typical for metals and many other solids (including binary semiconductors and complex phases [10]). In this case the precise *in situ* control and monitoring of incorporation process is possible under potentiostatic deposition mode. Electrode potential presents an instrument to fix oversaturation and, correspondingly, nucleation-growth conditions. As for monitoring, it is based on measuring current density and electric charge transients, providing information about nucleation-growth kinetics and filling degree. A number of complications arise when deposition is accompanied by parallel gas evolution process (i.e.

* Corresponding author. Tel.: +7 495 9395248; fax: +7 495 9390998.
E-mail address: napolsky@inorg.chem.msu.ru (K.S. Napolskii).
[1] ISE member.

0013-4686/$ – see front matter © 2010 Elsevier Ltd. All rights reserved.
doi:10.1016/j.electacta.2010.12.013

hydrogen evolution is unavoidable when depositing less noble metals). There is also a general problem: additional technological steps are required to arrange the electric contact at one side of template. This step is naturally well-taken when fabricating the arrays for applications requiring contacts.

The electrochemical deposition of nanowire arrays was first reported in 1970 [11], where tracked mica films were used as a template. Since then, this method has been successfully applied to prepare nanowires of metals [12,13], alloys [14], semiconductors [15], and conductive polymers [16,17] in various matrices with 1D channels.

Porous anodic aluminum oxide (AAO) films are known as a promising template for preparation of ordered arrays of nanowires. In comparison to other porous materials with 1D channels (such as track-etched membranes, porous silicon, block copolymer films, etc.), anodic alumina possesses well defined arrangement of pores, with structural parameters (pores diameter, interpore distance and membrane thickness) easily varied by tuning anodization conditions [18].

Nowadays, examination of homogeneity and completeness of the replication process in templates, is mostly addressed using scanning electron microscopy technique [14,19–21], which is known for its locality and can be applied only post factum. Small angle scattering techniques, such as small angle X-ray scattering, should also be mentioned as a useful tool giving an information about homogeneity of the filling, but these techniques are rather expensive (especially if applied *in situ* to monitor deposition) [22]. Despite electrodeposition approach is widely used for growth of various nanostructures in porous templates, its resources to monitor easily the replication process by electrochemical responses are still lacking. The examples of using current transients as indicators to reveal several stages of metal electrodeposition into the channels of track-etched membranes can be found in Refs. [23,24]. The rapid increase of current density occurs when the growth of hemispherical caps starts at external surface of porous template, i.e. when some faster growing nanowires reach this surface. Unfortunately, nearly no attention has been paid to a quantitative analysis of $j(t)$ curves and corresponding deposition charge. Our estimations based on the deposition charge data provided in Ref. [24] result in the filling factor below 50%.

In what follows we present the quantitative characterization of charge transients recorded in the course of potentiostatic deposition in combination with solid state characterization data. We demonstrate that this approach can shed a light to the growth process of metal nanostructures and allows us to find optimal deposition conditions. We observed that homogeneous filling of the porous films by nickel can be achieved only in a narrow range of deposition potentials (E_d): lower absolute values of potentials lead to very slow growth rates, while the higher rates result in a rapid decrease of pores filling factors. We also illustrate a profound effect of the deposition potential on the crystallinity and magnetic properties of Ni nanowire arrays.

2. Experimental

2.1. Samples preparation

The anodic alumina porous templates were prepared by two-step anodization technique [18]. Prior to anodization high purity aluminum foils (99.999%, 0.5 mm thick, Goodfellow) were annealed at 550 °C for 24 h in air in order to remove the mechanical stress and to enhance the grain size in the metal. Subsequently, the Al plates were mechanically polished by diamond suspensions (Struers) to a mirror finish and cleaned repeatedly with acetone and deionized water under sonication. The anodization was carried out in two-electrode cell in 0.3 M oxalic acid (98%, Aldrich) at constant applied potential difference of 40 V using Pt wire as a counter electrode. The electrolyte was pumped through the cell by a peristaltic pump, and its temperature was kept in the range of 2–4 °C during anodization. After first anodization for 48 h alumina film was selectively etched away in a 0.6 M H_3PO_4 + 0.2 M CrO_3 solution at 70 °C. After second anodization under the same conditions for 24 h, the ca. 50 μm thick oxide layers were obtained. Then the oxide films were separated from the aluminum substrate by selective metal dissolution in a mixture of Br_2 and CH_3OH (1:10 vol.). Subsequently, the pore bottoms were opened by chemical etching in a 5 vol.% H_3PO_4 aqueous solution at 60 °C for 5 min.

In order to prepare metal nanowire arrays by electrodeposition technique, a continuous layer of Au (ca. 100 nm thick) was thermally sputtered onto one side of the AAO template to serve as working electrode. Current densities and deposition charges per geometric surface area of this electrode are reported below. Copper plates were used as current collectors and mechanical supports for thin AAO/Au porous templates. Back side of working electrode was isolated with silicone wax. Electrodeposition of nickel was carried out in three-electrode cell from aerated 0.6 M $NiSO_4$ + 0.1 M $NiCl_2$ + 0.3 M H_3BO_3 electrolyte (pH 4.2) at room temperature. Platinum wire was used as a counter electrode. Saturated Ag/AgCl electrode connected with a cell via Luggin capillary served as the reference electrode. Potentials hereinafter are given versus saturated (KCl) Ag/AgCl electrode ($E_{Ag/AgCl} - E_{SHE} = 0.195$ V). Deposition was performed under potentiostatic mode controlled by Autolab PGSTAT 302 instrument in the potential interval $E_d = -0.7$ to -2.0 V.

In order to prevent the initial blocking of pores with air bubbles, vacuum pre-treatment procedure was carried out prior to metal electrodeposition [25].

2.2. Samples characterization

Electrochemical characterization of nanowires growth inside porous matrix was carried out by analysis of current transients recorded during electrodeposition using Autolab PGSTAT 302 potentiostat. All electrochemical experiments were performed in aerated electrolytes. Current efficiencies were determined by elemental analysis (Elan DRC II Perkin Elmer ICP mass spectrometer) of samples dissolved in hot aqua regia.

Scanning electron microscopy (SEM) images were recorded on a Supra 50 VP instrument (LEO). High resolution transmission electron microscopy (HRTEM) and selected-area electron diffraction measurements were performed using JEM-2100F (JEOL) instrument. The absence of the foreign phases in the prepared samples was confirmed by XRD analysis using the MAR diffractometer at the BM01A beam line (SNBL) at ESRF.

The magnetic properties of Ni/AAO nanocomposites were studied with a Cryogenics S-600 SQUID magnetometer.

3. Results and discussion

According to SEM observations, anodic alumina membranes prepared according to the abovementioned protocol possess a periodic hexagonal arrangement of pores with an average interpore distance $D_{int} \approx 105$ nm on a large area (Fig. 1). The AAO film has a narrow pore size distribution with an average pore diameter $D_p \approx 40$ nm. The cross-sectional image illustrates a constant pore diameter all over the thickness of AAO film (ca. 50 μm). The porosity of the AAO calculated from D_{int} and D_p equals 13%.

To estimate the Ni deposition potential range, cyclic voltammetry measurements were performed in 0.6 M $NiSO_4$ + 0.1 M $NiCl_2$ + 0.3 M H_3BO_3 electrolyte (pH 4.2) using gold plate as a working electrode (Fig. 2(a)). An equilibrium potential for nickel in this

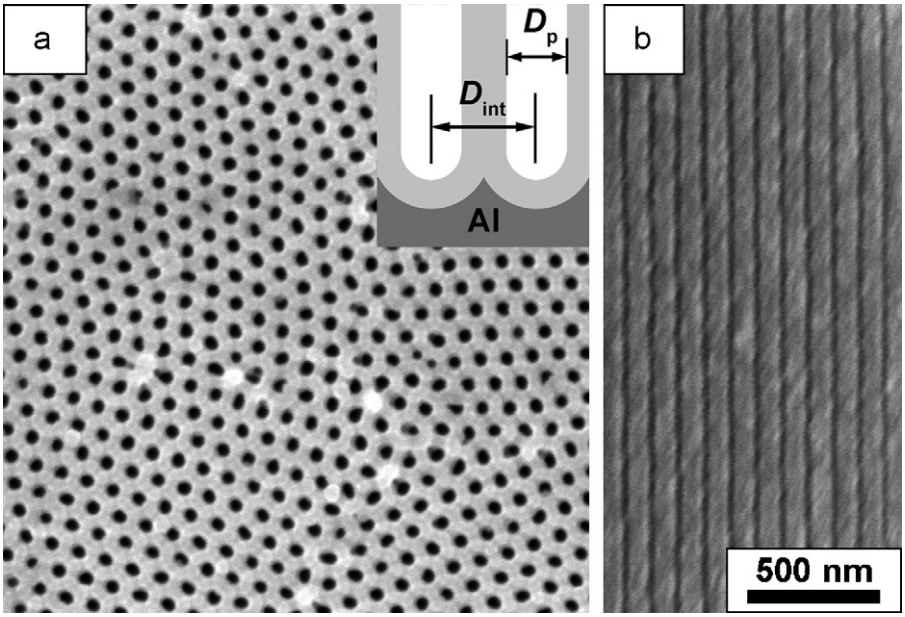

Fig. 1. SEM images of AAO porous film: top view (a) and cross-section (b). The inset shows the schematic cross-section of the porous alumina structure: D_{int} is interpore distance, D_p is pore diameter.

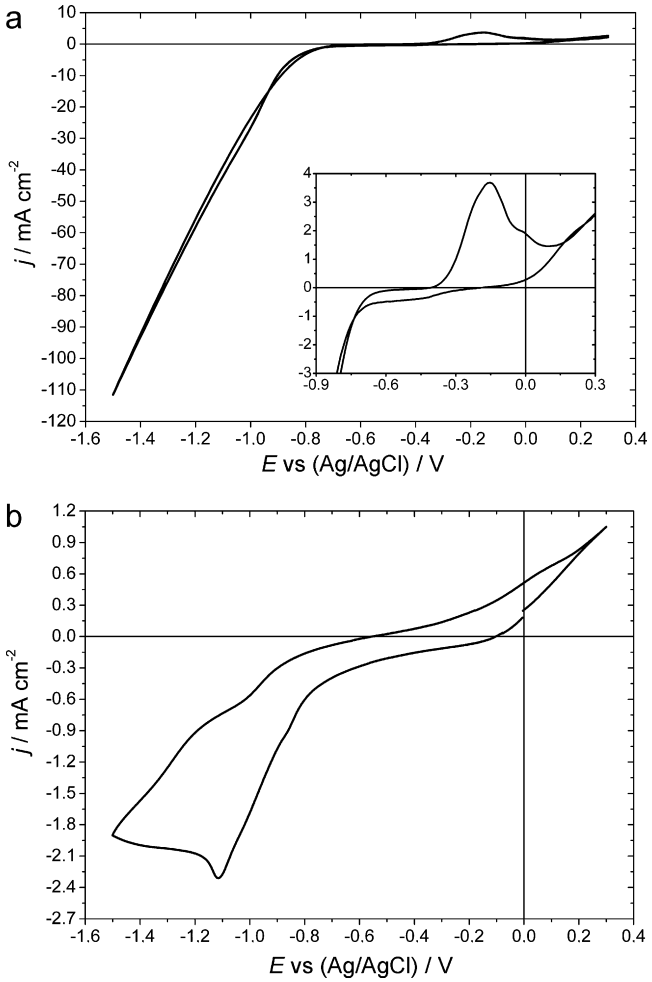

Fig. 2. Cyclic voltammograms recorded for 0.6 mol dm^{-3} $NiSO_4$ + 0.1 mol dm^{-3} $NiCl_2$ + 0.3 mol dm^{-3} H_3BO_3 on a bare Au plate (a) and on AAO/Au porous electrode (b) at 20 mV s^{-1}. The inset on panel (a) presents the enlarge part of voltammogram in the region from −0.9 to 0.3 V.

solution can be roughly estimated as −0.46 V (unfortunately the activity of nickel ions remains unknown). A low current plateau was found for potentials higher than −0.7 V indicating a very low Ni deposition rate under this mode. At more negative potentials current density increases, and a typical "nucleation loop" is noticeable. The dissolution of Ni is observed at the potentials above −0.3 V. All voltammetric features and characteristic potential intervals are very similar to voltammetric details reported earlier for Watts type electrolytes [26].

In case of AAO working electrode the picture changes drastically (Fig. 2(b)). The voltammogram indicates a broad maximum at −1.2 V, and no loop is observed. Current density is ca. 50 times lower as compared to deposition on bare Au support. Thus the decrease of current when going from bare to partly screened surface is much stronger than the simultaneous decrease of electrochemically available surface area (<10 times). This difference can be assigned to much slower diffusion of Ni^{2+} through nanochannels to metal/electrolyte interface and, correspondingly, to higher diffusion contribution to mixed deposition current. Manifestations of higher Ohmic drop are also evident, induced by high solution resistance in very thin pores, hence some distortion of potential values is unavoidable, especially at high deposition currents. The deposition rate at saturation conditions ($E < -1.2$ V) can be calculated from Faraday's law according

$$\frac{d\upsilon}{dt} = \frac{\eta}{nFS_{pores}}\frac{dq}{dt} \quad (1)$$

η is current efficiency, $n = 2$, F is Faraday constant (96,500 C mol^{-1}), q is charge density per geometric surface area, and S_{pores} is a relative electrochemically available surface area in AAO film. The dimensionless value of S_{pores} for anodic alumina film is equal to its porosity, and can be easily obtained from the geometric parameters of the structure: for 40 nm pores and pore density of 1.05×10^{10} cm^{-2} $S_{pores} = 0.13$. Experimental current efficiencies were obtained by elemental analysis of samples electrodeposited at constant potential. Using $\eta \approx 0.5$ for E form −1.5 to −1.2 V one can evaluate the metal growth rate as $\sim 4.0 \times 10^{-8}$ mol cm^{-2} s^{-1}.

From the other hand a flux of Ni_{aq}^{2+} from the solution to electrode can be very roughly estimated by applying Fick's law $j = -D\nabla C = D(C_{electr} - C_{ext})/d$ with C_{ext} equals to Ni_{aq}^{2+} concen-

tration in electrolyte volume, $C_{electr} \ll C_{ext}$, and d equals to AAO layer thickness. To find the order of magnitude, not the value, we assume steady-state diffusion to planar surface. We also neglect the role of electroosmotic and convectional flow (taking into account the blocking of pores basements by the support, as well as small pore diameter). Electromigration of nickel ions can play a certain role, however it is also negligible due to a high concentration of electrolyte and low electric field applied during electrodeposition. Therefore the main contribution to Ni_{aq}^{2+} flux goes from chemical diffusion. One should also take into account that an effective diffusion of cations in AAO channels is suppressed as compared to bulk diffusion, because of the positive charge of the alumina surface in acidic medium [27–29].

To prove this suggestion we have performed a direct measurement of Ni_{aq}^{2+} flux through AAO membrane with a thickness of 50 μm under electric field. The AAO membrane with through pores was fixed in a H-cell filled by 20 ml of electrolyte for nickel electrodeposition from one side, and by 20 ml of indifferent electrolyte of close ionic strength (0.6 M Na_2SO_4 + 0.2 M NaCl + 0.3 M H_3BO_3) from another (permeate) side. Working and counter electrodes were placed into Ni-containing and Ni-free solutions correspondingly. The potential of −1.0 V versus saturated Ag/AgCl electrode was applied. Nickel concentration in permeate was directly measured by ICP mass spectrometry. These measurements gave a value of Ni_{aq}^{2+} diffusion flux of 2.8×10^{-8} mol cm^{-2} s^{-1}, which stays rather close to nickel growth rate estimated from the current density. The above mentioned calculations were performed under assumption of all pores being involved in the transport process. Thus the estimated nickel ions flux should be considered as the lower limit of Ni_{aq}^{2+} flux through single pore.

The calculated diffusion coefficient of Ni_{aq}^{2+} in AAO channels ($\sim 2.0 \times 10^{-7}$ cm^2 s^{-1}) is found to be far less than bulk diffusion coefficient of nickel in aqueous solutions ($\sim 0.6 \times 10^{-5}$ cm^2 s^{-1}) [30]. According to literature [27] this fact is attributed to suppression of diffusion by electric double layer in nanochannel.

One should note that high potentials can also result in blocking of pores by hydrogen gas generated inside the pores. Indeed, at potentials above −1.2 V hydrogen generation is clearly visible with unaided eye. Basing on cyclic voltammetry results the potential range starting from −0.7 V was chosen for a detailed examination of the electrodeposition potential effect on the microstructure and morphology of Ni nanowires grown in AAO templates.

Fig. 3(a) demonstrates a typical current transient recorded in the course of potentiostatic metal deposition into porous AAO membrane. There are several characteristic stages of electrodeposition process [23]. At first, maximum of cathodic current corresponding to nucleation process is observed (region I, see insert as well) followed by a nearly steady-state regime of electrodeposition at constant current on the second stage, which corresponds to nickel growth within AAO channels (region II). Next at a third stage, a rapid current increase occurs, indicating nanowires approaching anodic film surface and growth of hemispherical caps at the end of each wire (region III). Expansive growth of metal surface at this stage turns into coalesce of hemispherical caps to form planar and contiguous metallic top layer. Growth of metallic layer at the fourth stage takes place at a constant current (region IV).

To provide an accurate analysis of metal deposition process, current efficiencies (η) were calculated for Ni electrodeposited into AAO templates at various potentials. Total quantities of nickel in Ni/AAO nanocomposites were determined by elemental analysis of samples dissolved in hot aqua regia. Current efficiencies of 82–87% were found for −0.8 to −1.1 V interval, in satisfactory agreement with current efficiency for galvanostatic nickel deposition on bare supports under usual galvanostatic modes known from galvanics. At more negative potentials, the efficiencies fall down and reach ca. 10% at −2.0 V. This means that when Ni nucleation in some pores is blocked, hydrogen evolution continues at this portion of electrode surface.

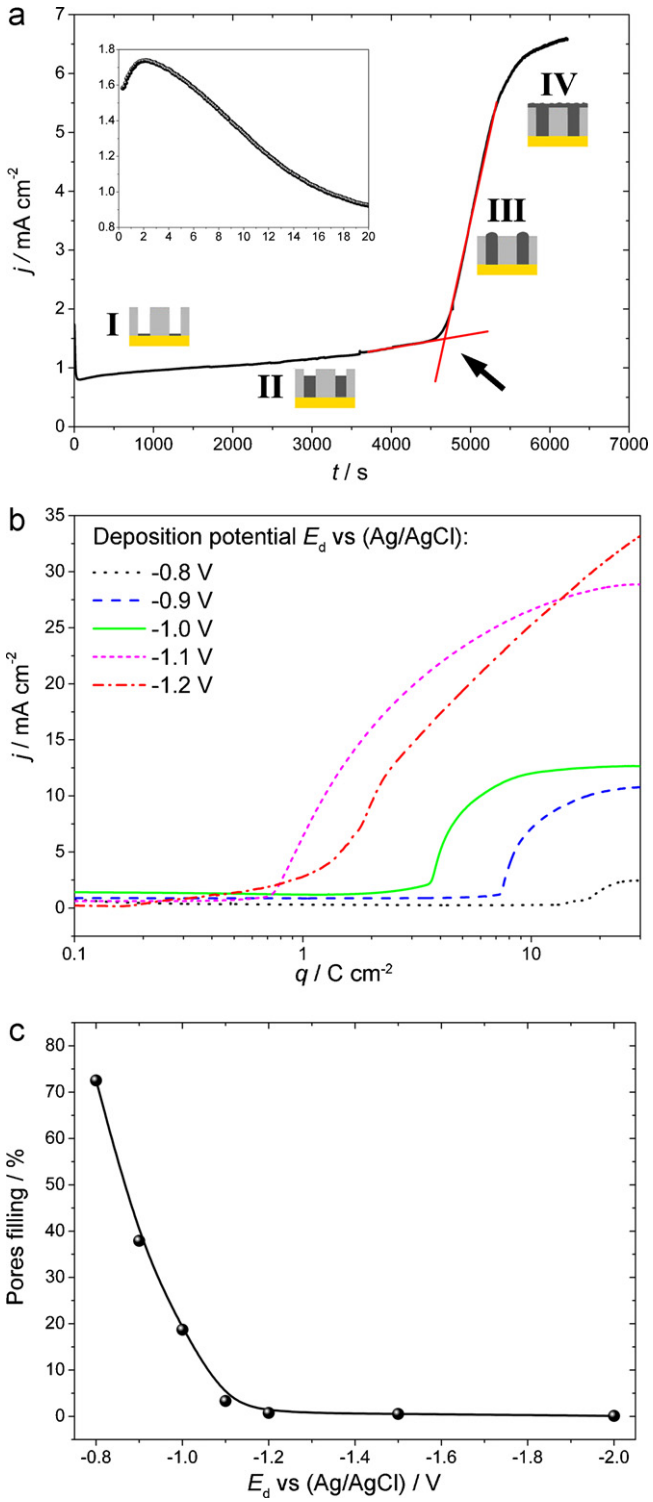

Fig. 3. Time (a) and charge (b) dependences of Ni electrodeposition current (potentiostatic mode) for AAO/Au porous template. The inset in panel (a) shows initial region of j–t curve. I–IV correspond to deposition stages. Arrow indicates the transition from II to III deposition stages. The curves obtained at various deposition potentials (b), as well as the degree of pores filling (c), are presented after correction for current efficiency.

It should be noted that both duration and current densities at different stages of electrodeposition depend strongly on the applied potential. Fig. 3(b) illustrates a plot of current densities

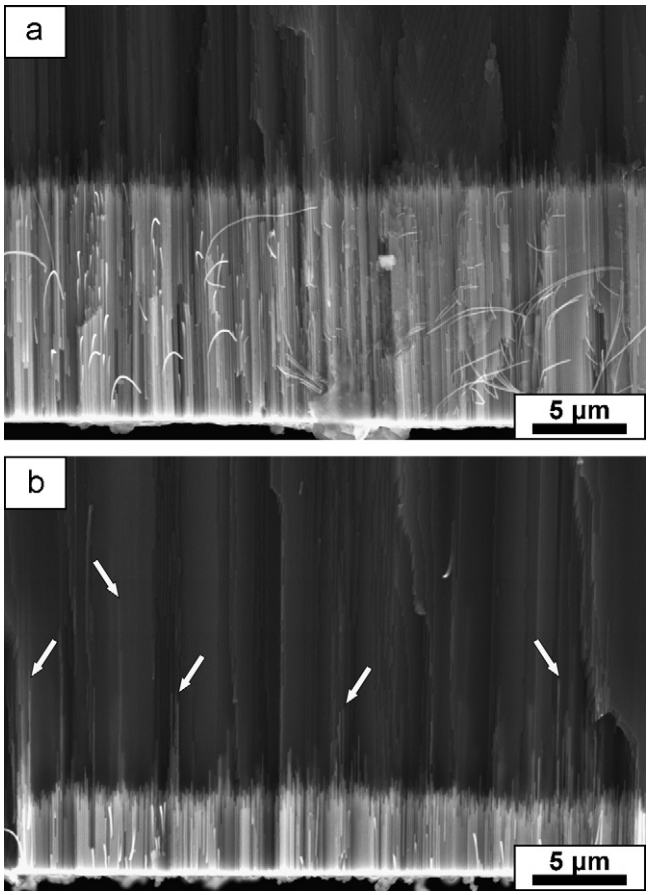

Fig. 4. SEM images of cross-sections of Ni/AAO nanocomposites obtained at various deposition potentials E_d: (a) −0.8 V, (b) −1.2 V. Deposition charge equals 10 and 9 C cm^{-2} for samples presented on panel (a) and (b), respectively. Arrows in (b) show the rare wires being much longer than the majority of growing nanostructures.

as a function of electric charge spent for metal deposition. Here and below current density is corrected to the current efficiency. One can clearly see that the charge spent before the moment when nickel nanowires approach the external surface of AAO (transition from region II to region III) decreases gradually with the shift of electrodeposition potential to more negative values (Fig. 3(c)). Thus, the potential affects not only current density (that is equivalent to the growth rate), but also metal loading value. In particular, the potential change from −0.8 to −0.9 V leads to the reduction of the charge passed till the moment of metal growth at the membrane surface nearly twice from 13.7 to 7.2 C cm^{-2}. This interval of the least negative potentials at which we were able to deposit Ni with a reasonable rate is close to potential interval studied in classical Fleischmann's work [31]. According to [31], in this region nickel deposition on a flat support takes place under kinetic control, when in our membrane configuration mixed currents are more probable, because of slow diffusion inside the pores.

The electric charge necessary for homogeneous filling of all the AAO pores by nickel (at $\eta = 1$) can be valued by Faraday's law:

$$q_{\text{theor}} = \frac{nF\rho V}{M} \quad (2)$$

where $\rho = 8.9$ g cm^{-3}, $M = 59$ g mol^{-1} are density and atomic weight of nickel and V is the volume of the pores. For 50 μm thick film with 40 nm pores and a pore density of 1.05×10^{10} cm^{-2} the expected charge equals 18.9 C cm^{-2}, which is notably higher than the experimental values. An analysis of the pores filling factors ($q_{\text{exp}}/q_{\text{theor}}$), clearly indicates the tendency of rapid decrease of nickel loading at deposition potential shift from −0.8 V to more negative values (the trend is illustrated in Fig. 3(c)). Therefore to provide homogeneous filling of pores by metal one needs to apply less negative potential, but still corresponding to reasonable growth time. In our experiments it is surely −0.8 V, not −0.7 V because of too low growth rate in the latter case.

An analysis of growth front homogeneity by SEM imaging of Ni/AAO composites cross-sections illustrates more or less uniform growth of nickel wires in different pores if the potential is not too negative (Fig. 4(a)), i.e. the majority of pores are filled simultaneously with close rates. Under these favorable deposition conditions the length of nanowires depends directly on the electric charge and can be varied controllably by Faraday law. On the other hand, as the total charge spent before the moment when nanowires approach the surface depends pronouncedly on deposition potential, we should conclude that electrodeposition does not take place in a number of pores, which stay partly or totally unfilled (either from the very beginning, or starting from some moment after initial growth of a short wire). This may happen by a number of reasons. First, for very small channels the nucleation fails to start due to absence of active sites or blocking of metal/electrolyte contact by an air persistent in the pores and not deleted before the deposition. Second, the growth can stop at the early stage if the reagent diffusion to gold electrode is limited by pore coning/narrowing at some point. Third, at high negative potential the growth of nanowire can be eventually stopped at any moment due to the blocking of pore by a hydrogen bubble. An efficiency of all these process (especially diffusion and hydrogen generation) depends significantly on the applied potential, thus leading to an essential decrease of metal loading. This is clearly seen in Fig. 4(b), where the majority of wires are still very short, when some certain wires (see arrows) are already many times longer. This inhomogeneity of the growth front correlates with the portion of completely empty pores and explains why the filling factor can be below 1% even when the metallic layer already starts to grow at the external surface.

According to TEM studies of samples after matrix dissolution, all of them consist of metal nanowires with diameters very close to channel diameter in AAO template (Fig. 5). However the crystallinity of nanowires from different samples was found to be completely different. At low overpotentials the wires have polycrystalline structure, in the middle potential range of −0.9 to

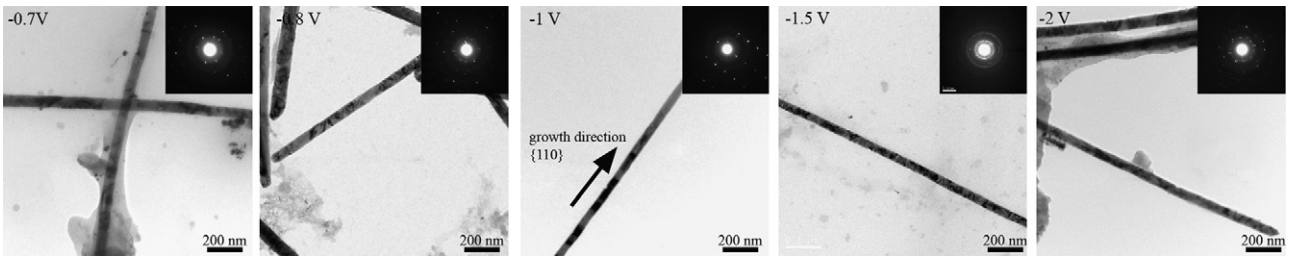

Fig. 5. TEM images of Ni nanowires extracted from the oxide matrix. Insets present selected area electron diffraction patterns recorded from single nanowires.

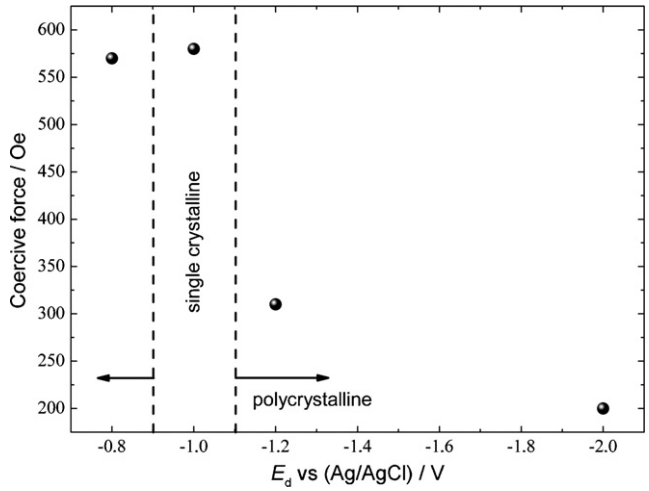

Fig. 6. Dependence of the coercivity of Ni/AAO nanocomposites in longitudinal direction on deposition potential.

−1.2 V single crystalline wires are formed, while higher overpotentials again lead to polycrystalline wires formation. One can note that the tendency for crystallinity is similar to the trend for current efficiencies. Indeed as $Ni^{2+} \rightarrow Ni$ and $2H^+ \rightarrow H_2$ reactions take place simultaneously at the metal/electrolyte interface, they should be considered as concurrent processes. The oxygen reduction process $O_2 + 4H^+ \rightarrow 2H_2O$ can also play a role, especially at low absolute values of deposition potential, as we are dealing with aerated solutions. In case $Ni^{2+} \rightarrow Ni$ is dominant one the continuous single-crystalline wires are formed, while in case of the advantage of $2H^+ \rightarrow H_2$ process hydrogen microbubbles form on metal/electrolyte interface resulting in secondary nucleation of nickel and polycrystalline nanowire structure. Additional factor of structural disorder can be nickel hydride formation [32], with subsequent withdrawal of hydrogen in air. For pH above 2 concentrated β-hydride is expected to form only at very high negative potentials. We can assume that non-monotonous trend observed for polycristallinity results also from the adsorption of anionic reacting species (Ni(II) aquachloride complexes). This phenomenon can be strongly affected by the electrode charge, and can support the formation of additional nucleation centers.

Crystalline structure of metal nanowire influences effectively the functional properties of Ni/AAO composites. In particular the coercivity of Ni/AAO in longitudinal direction falls more than twice when going from single-crystalline to polycrystalline structures (Fig. 6). One should note that the effect cannot arise from magnetic dipole interactions between the neighboring wires, as magnetostatic interactions are known to decrease with distance as l^{-3} in the direction perpendicular to magnetic dipole orientation [1]. This indicates a decrease of an interaction field with decreasing pore filling factors, which is contrary to the observed tendency. On the other hand grain boundaries in nanowire can act as magnetic reversal nucleation sites, leading to sharp decrease in coercive force and remanence magnetization by decreasing demagnetization field [1]. Thus the magnetic properties are more sensitive to the crystallinity of nanowires than to filling factors, leading to sharp decrease of nanocomposite coercivity with increasing metal deposition overpotential.

4. Conclusions

The quantitative coulometric analysis of current transients recorded in the course of potentiostatic deposition of metals into the pores of anodic aluminum oxide characterizes inclusively a deposition process and the structure of Ni/AAO nanocomposites. The complete and homogeneous filling of the porous template with nickel can be achieved only in a narrow range of deposition potentials: lower deviations from equilibrium potential lead to very slow growth rates, while more negative potentials result in a rapid decrease of pores filling factors. The deposition potential also defines the crystallinity and magnetic properties of Ni nanowire arrays.

Our attempts to obtain the initial regions of current transients (region I) reproducibly, in order to analyze nucleation kinetics, were less successful at this stage. Most probably the reason is nucleation statistical nature, as the size of bottom of a single pore can correspond to very few nucleation centers. One cannot also exclude less reproducible blocking with the residual air and/or initially formed hydrogen bubbles. Surprisingly, despite of this very arbitrary nucleation behavior the potential-dependent growth of metal in the regions II and III is quite reproducible if the potential is not too negative.

Monitoring mentioned above in Introduction can be arranged in the form of plots presented in Fig. 3(b). These plots provide the reliable information about pores filling in a wide potential range, in which current efficiency remains constant. As for controllability, it is the highest for very narrow potential interval supporting more or less homogeneous growth front.

Acknowledgments

This work is partially supported by the Russian Ministry of Education and Science (grants nos. 02.513.11.3485 and 14.740.11.0301), the Russian Foundation for Basic Research (grants nos. 09-03-01123, 09-03-12246 and 10-02-00634) and RF President Grant MK-6626.2010.3. The authors are grateful to D.Yu. Chernyshov (ESRF) for his help with XRD analysis.

References

[1] L. Sun, Y. Hao, C.-L. Chien, P.C. Searson, IBM J. Res. Dev. 49 (2005) 79.
[2] K. Nielsch, R.B. Wehrspohn, J. Barthel, J. Kirschner, U. Gosele, S.F. Fischer, H. Kronmuller, Appl. Phys. Lett. 79 (2001) 1360.
[3] V.N. Tondare, B.I. Birajdar, N. Pradeep, D.S. Joag, A. Lobo, S.K. Kulkarni, Appl. Phys. Lett. 77 (2000) 2394.
[4] K.F. Huo, Y.M. Hu, J.J. Fu, X.B. Wang, P.K. Chu, Z. Hu, Y. Chen, J. Phys. Chem. C 111 (2007) 5876.
[5] J.S. Suh, J.S. Lee, Appl. Phys. Lett. 75 (1999) 2047.
[6] O.K. Varghese, D.W. Gong, M. Paulose, K.G. Ong, C.A. Grimes, E.C. Dickey, J. Mater. Res. 17 (2002) 1162.
[7] H. Chik, J.M. Xu, Mater. Sci. Eng. R 43 (2004) 103.
[8] K. Kordas, G. Toth, J. Levoska, M. Huuhtanen, R. Keiski, M. Harkonen, T.F. George, J. Vahakangas, Nanotechnology 17 (2006) 1459.
[9] X.P. Shen, A.H. Yuan, F. Wang, J.M. Hong, Z. Xu, Solid State Commun. 133 (2005) 19.
[10] M. Lai, D.J. Riley, J. Colloid Interface Sci. 323 (2008) 203.
[11] G.E. Possin, Rev. Sci. Instrum. 41 (1970) 772.
[12] D. Almawlawi, N. Coombs, M. Moskovits, J. Appl. Phys. 70 (1991) 4421.
[13] L. Piraux, S. Dubois, S. Demoustier-Champagne, Nucl. Instrum. Methods Phys. Res. B 131 (1997) 357.
[14] S.Z. Chu, S. Inoue, K. Wada, K. Kurashima, Electrochim. Acta 51 (2005) 820.
[15] D. Routkevitch, T. Bigioni, M. Moskovits, J.M. Xu, J. Phys. Chem. 100 (1996) 14037.
[16] C.W. Wang, Z. Wang, M.K. Li, H.L. Li, Chem. Phys. Lett. 341 (2001) 431.
[17] M. Delvaux, J. Duchet, P.Y. Stavaux, R. Legras, S. Demoustier-Champagne, Synth. Met. 113 (2000) 275.
[18] H. Masuda, M. Satoh, Jpn. J. Appl. Phys. 35 (1996) L126.
[19] R. Inguanta, S. Piazza, C. Sunseri, Electrochim. Acta 53 (2008) 5766.
[20] G.J. Strijkers, J.H.J. Dalderop, M.A.A. Broeksteeg, H.J.M. Swagten, W.J.M. de Jonge, J. Appl. Phys. 86 (1999) 5141.
[21] V. Haehnel, S. Fahler, P. Schaaf, M. Miglierini, C. Mickel, L. Schultz, H. Schlorb, Acta Mater. 58 (2010) 2330.
[22] R.E. Benfield, D. Grandjean, J.C. Dore, H. Esfahanian, Z. Wu, M. Kroll, M. Geerkens, G. Schmid, Faraday Discuss. 125 (2004) 327.
[23] T.M. Whitney, J.S. Jiang, P.C. Searson, C.L. Chien, Science 261 (1993) 1316.
[24] M. Motoyama, Y. Fukunaka, T. Sakka, Y.H. Ogata, S. Kikuchi, J. Electroanal. Chem. 584 (2005) 84.
[25] K.S. Napolskii, P.J. Barczuk, S.Yu. Vassiliev, A.G. Veresov, G.A. Tsirlina, P.J. Kulesza, Electrochim. Acta 52 (2007) 7910.

[26] G.R.P. Malpass, M. Kalaji, E.C. Venancio, A.J. Motheo, Electrochim. Acta 49 (2004) 4933.
[27] E.A. Bluhm, E. Bauer, R.M. Chamberlin, K.D. Abney, J.S. Young, G.D. Jarvinen, Langmuir 15 (1999) 8668.
[28] E.A. Bluhm, N.C. Schroeder, E. Bauer, J.N. Fife, R.M. Chamberlin, K.D. Abney, J.S. Young, G.D. Jarvinen, Langmuir 16 (2000) 7056.
[29] R. Schmuhl, K. Keizer, A. van den Berg, J.E. ten Elshof, D.H.A. Blank, J. Colloid Interface Sci. 273 (2004) 331.
[30] R.H. Stokes, S. Phang, R. Mills, J. Solution Chem. 8 (1979) 489.
[31] A. Sarabyreintjes, M. Fleischmann, Electrochim. Acta 29 (1984) 557.
[32] M. Monev, Electrochim. Acta 46 (2001) 2373.